Quaternary Science Reviews 78 (2013) 369–380

Contents lists available at SciVerse ScienceDirect

Quaternary Science Reviews

journal homepage: www.elsevier.com/locate/quascirev

Initiation and variation of the dune fields in semi-arid China – with a special reference to the Hunshandake Sandy Land, Inner Mongolia

Xiaoping Yang [a,*], Xulong Wang [b], Ziting Liu [a], Hongwei Li [a], Xiaozun Ren [a], Deguo Zhang [a], Zhibang Ma [a], Patrick Rioual [a], Xindi Jin [a], Louis Scuderi [c]

[a] Key Laboratory of Cenozoic Geology and Environment, Institute of Geology and Geophysics, Chinese Academy of Sciences, P.O. Box 9825, Beijing 100029, China
[b] Institute of Earth Environment, Chinese Academy of Sciences, Xian 710075, China
[c] Department of Earth and Planetary Sciences, University of New Mexico, MSC03 2040 Albuquerque, NM 87131, USA

ARTICLE INFO

Article history:
Received 8 March 2012
Received in revised form
30 January 2013
Accepted 1 February 2013
Available online 21 March 2013

Keywords:
Desert
Palaeosol
Aeolian system
Sand dune
Climate change
Holocene
Pleistocene
Middle latitude
Hunshandake
China

ABSTRACT

Sedimentary sequences occurring in desert dunes reflect changes in desert systems, and as such may contain signals useful for recognizing spatial and temporal changes of deserts and their response to regional or even global climate fluctuations. Geomorphological and palaeoenvironmental studies within the dune fields of the Asian middle-latitudes have provided some solid evidence for interpreting the history of these sand seas. Using the Hunshandake (Otindag) Sandy Land, a sandy area covered primarily by stabilized dunes and located in the semi-arid zone of eastern Inner Mongolia, China (Fig. 1), as an example, we studied the initiation and variation in the dune landscape in the eastern portion of the desert belt in northern China. On the basis of physical and biochemical indicators in the sediments and OSL chronology, we herein argue that this dune system in the middle latitudes of eastern Asia is much younger than previously assumed and that it has responded sensitively to climate change during the late Quaternary. Geological evidence from the Sandy Land suggests that most of the current dunes are of late Pleistocene or even Holocene age. Palaeosols intercalated in the aeolian sequences and their OSL chronology show that the climate of the Hunshandake was much wetter than today between 9.6 ka and 3 ka. This resulted in stabilization of the dunes in the eastern and central portions of the Sandy Land. Epochs of reworking or stabilization of the dunes are broadly consistent with the fluctuations in northern hemisphere solar radiation although with an obvious time lag. Because the increase rate of annual precipitation was not sufficient to fully stabilize the dunes in more arid part of the region, some active dunes persisted even during this long-lasting wetter epoch. We conclude that periods of Holocene dune stabilization due to palaeosol formation varied along the climate gradients across the various sandy lands of northern China, and in general it began earlier and lasted longer in the east than in the west. The general nature of the sandy lands and their counterparts in the western portion of the desert belt during the LGM and mid-Holocene climate optimum is discussed in comparison with their current states.

1. Introduction

Northern China exhibits distinct variations in climate and vegetation resulting in variation in the size and form of dune fields (Yang et al., 2012). Dune fields of the eastern portion of the mid-latitude deserts in Asia can be divided into two primary types – sand seas located in the arid western portion and sandy lands in the semi-arid eastern portion (Zhu et al., 1980). Fields of dunes stabilized by vegetation in the sandy lands of northern China are under the combined influence of the East Asian Monsoon (EAM) and Northern Hemisphere Westerlies (NHW). The response of different climate components varies locally depending on location relative to these two climatic drivers (Wu et al., 2007; Dallmeyer et al., 2010). As well, clear spatial differences in the timing of maximal precipitation during the Holocene have been attributed to variable contribution of the EAM (An et al., 2000). Due to the great heterogeneity of climates and landscapes within the vast desert belt of northern China (Ren, 1980; Zhu et al., 1980; Derbyshire and Goudie, 1997), atmospheric response to orbital forcing and the strength of feedbacks from these forcings likely differ from region to region. It is therefore of great importance to examine the palaeoclimatic history of each region along the desert belt in order to provide a comprehensive understanding of the environmental change that occurred within the different climate systems.

* Corresponding author. Tel.: +86 1082998387.
E-mail addresses: xpyang@mail.igcas.ac.cn, xpyang@263.net.cn (X. Yang).

0277-3791/$ – see front matter © 2013 Elsevier Ltd. All rights reserved.
http://dx.doi.org/10.1016/j.quascirev.2013.02.006

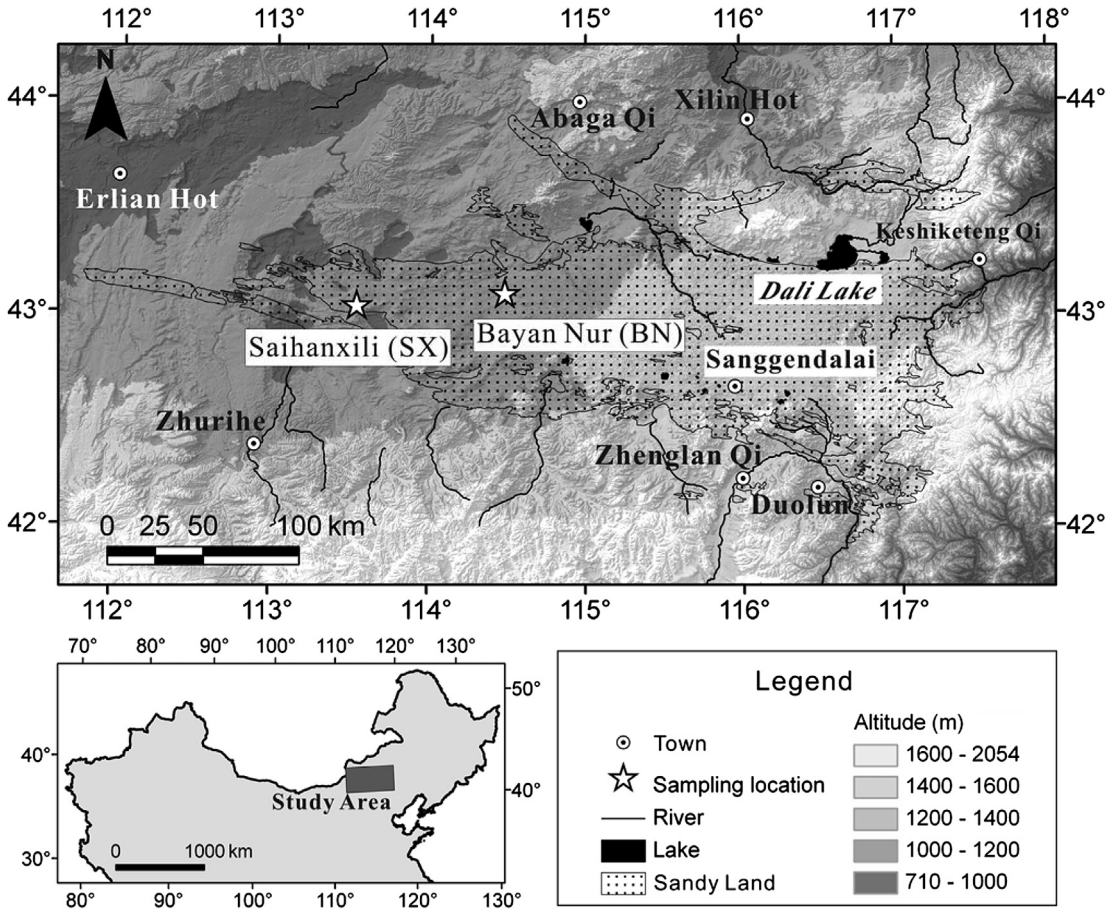

Fig. 1. Study area location.

Since these deserts are geographically located in the northern margin of the influence of the East Asian summer monsoon, and at the eastern edge of westerly flow over the Eurasian continent, they are likely highly sensitive to small shifts in the location and intensity of these climatic drivers. Knowledge of the palaeoenvironmental history of the deserts is therefore crucial to the reconstruction of late-Pleistocene and Holocene EAM and NHW variability. Due to their ecologically sensitive nature and well known input to global dust loadings and biogeochemical cycles (Goudie, 2002; Tooth, 2008), study of these deserts can also provide crucial palaeoenvironmental evidence needed to test and to adjust palaeoclimatic simulations and to estimate the contributions these arid and semi-arid regions have had during periods of climatic change.

Earlier studies, primarily based on the differences in colour between palaeosols and aeolian sand layers in the aeolian sequences, have shown that significant change in climate has occurred in the sandy lands of northern China. However, opinions on the timing and intensity as well as triggering factors of this change are different and at times even contradictory (e.g., Zhu et al., 1980; Zhu and Liu, 1981; Zhu and Chen, 1994; Sun et al., 1998; Lu et al., 2005; Li and Sun, 2006; Zhao et al., 2007; Mason et al., 2008, 2009; Yang et al., 2008, 2011; Yang and Scuderi, 2010; Wang et al., 2011). The aims of this paper are therefore to identify major change in the sedimentary sequences of these deserts, to illustrate Holocene climatic variation in this sensitive region on the basis of interpreting multiple proxies of the sedimentary record of intercalated aeolian sands and palaeosols, and from this to infer knowledge about the initiation and development of the desert landscape in the semi-arid regions of northern China. Finally, by comparing records from Hunshandake with studies in other Chinese deserts we show patterns of Late Quaternary desert landscape change in China and their possible response to the past global climate change.

2. Regional setting

Hunshandake Sandy Land (~21,400 km^2), ranging from 1500–2000 m above sea level (asl.) in the southeast to about 1000 m asl. in the northwest, is bordered by flat steppe terrain to the north and mountainous loess landscape to the south (Fig. 1). The Sandy Land sits on the flat floor of a graben formed during the Palaeozoic (Wang, 2003). Climatically, the area belongs to the temperate semi-arid zone with cold winters and warm summers.

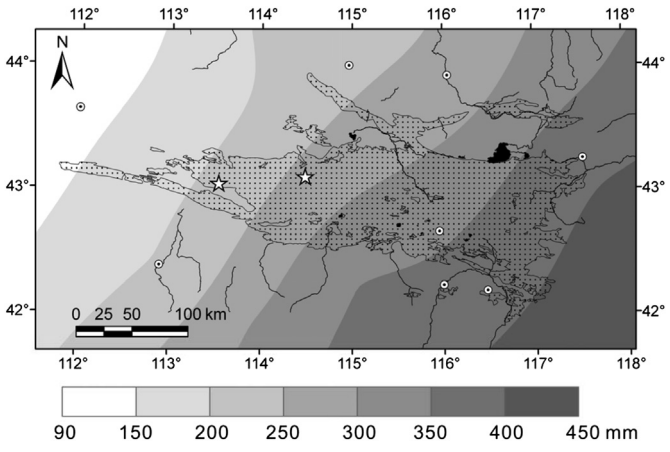

Fig. 2. Mean annual precipitation in the study area.

Based on Köppen's classification system (Köppen, 1931; Domrös and Peng, 1988) the eastern part of the sandy land belongs to the BSk climate while the western part to the BWk. The mean monthly temperature is ~ −20 °C in January +20 °C in July. Due to the decreasing influence of the East Asian summer monsoon from southeast to northwest, the mean annual rainfall is ~450 mm in the southeast and decreases to ~150 mm in the northwest (Fig. 2). Mostly complete wind records from the past three decades show that the dominant winds capable of moving sand are primarily from northwest and west in all seasons except summer (Fig. 3), and are predominantly the result of the strong Asian winter monsoon and northern hemispheric westerly flow patterns.

Dunes in the Sandy Land are barchans, parabolic, linear and grid-formed (or network dunes employed in Warren, 1988) types, ranging from a few metres to over 40 m in height (Zhu et al., 1980; Mason et al., 2008; Yang et al., 2008). The windward side of the dunes is often characterized by bare sand surfaces or deflation pits while the leeside is mostly stabilized by vegetation. However, active sand deposition can occur on the slip faces at the leeward sides of all kinds of dunes. This vegetation cover strongly controls dune forms. The predominant plants in the Sandy Land are grasses of the family Poaceae and are suitable for animal-grazing. Other vegetation includes shrubs such as *Artemisia* and *Salix microstachya*, and trees like *Ulmus*, *Pinus* and *Betula*.

3. Methods

Fieldwork was carried out in the central and western parts of the Hunshandake Sandy Land, primarily along dirt roads linking the residential sites of local herdsmen. Geomorphological and stratigraphical mapping was augmented by topographical maps 1:50,000, Google Earth™ imagery and by GPS positioning. Palaeosols and aeolian, lacustrine/fluvial sediments were identified based on bedding, colour, texture and carbonate content. Boundaries between horizons in the sections were marked at points where a significant sharp transition occurred between the different layers or, when the boundary was transitional in nature, at the midpoint of the transition.

Recent road construction resulted in the excavation of many deep quarries with vertical walls that provided us with the opportunity to observe both vertical and horizontal sediment variation. Two particularly well-exposed quarry sites, Saihanxili (SX) and Bayan Nur (BN) were selected for detailed investigation (Fig. 1). The area surrounding both sections is characterized by a nearly continuous thin vegetation cover, suggesting that the plants protect the sites from intensive deflation. The SX section is in a large inter-dune basin while the BN section is located on the west side of a large lacustrine basin where only a shallow lake occurs at present (the section site is ca 25 m above current lake level). This lake basin is currently encircled by stabilized dunes. Sediment samples were taken from cleaned pit walls (original road cuts were further trenched during our field work) at 10 cm intervals and those used in OSL dating were obtained by hammering steel tubes into the wall with careful consideration given to the changes in sedimentary facies.

The samples were dated in the Laboratory of OSL Chronology, Institute of Earth Environment, Chinese Academy of Sciences (CAS) in Xian. Well-sealed sample tubes were processed under subdued red light, with sand from the central part of the tube used for isolation of quartz for OSL dating. Sediments used to determine the equivalent dose (*De*) were first treated with 10% hydrochloric acid and 30% hydrogen peroxide to remove carbonate and organic matter, and then wet sieved to obtain the 90–125 μm grain fraction. This fraction was etched by 30% hydrofluorosilicic acid, subsequently isolated by density separation, and finally sieved again. The purity of coarse quartz was examined by IR stimulation.

Luminescence measurements of all quartz aliquots were derived in an automated Daybreak 2200 TL/OSL reader with a $^{90}Sr/^{90}Y$ beta source for irradiation. Optical stimulation with blue LEDs (470 ± 5 nm) was performed at 125 °C, and OSL emission was detected through two 3 mm of U-340 glass filters. *De* values of the grains were determined by Single-aliquot Regenerative-dose (SAR) protocol (Murray and Wintle, 2000). Preheating conditions were 260 °C (10 s) and 220 °C (10 s) for natural/regeneration OSL (Li) and test dose OSL (Ti) responses, respectively. The OSL signal from the first 5 s and subtracted that from the last 5 s of the decay curve were applied to construct dose regenerative growth curve of the corrected OSL intensity (Li/Ti) and to determine the equivalent dose (*De*) value. The recycling ratio for all samples was close to 1, and the zero dose recuperation ratio was less than 5%. With respect to the *De* value distribution of a sample related to the bleaching history, a mean of *De* values from the well-bleached aliquots was used to estimate the age of the sample.

The sand at the two ends of the sample tube was used to determine the uranium and thorium concentrations by ICP-MS, and the K content using the ICP-OES method. The analytical uncertainties (relative standard deviation) are less than ±1% for measuring K and less than ± 3% for uranium and thorium, respectively. Bearing in mind that the wetness may have changed during the burial time, dose rate was calculated using the conversion factors (Adamiec and Aitken, 1998), assuming that all samples had an average water content of 10% during burial (an error of 5% was assumed for all samples). The contribution of cosmic rays to the dose rate was calculated applying current depth (Prescott and Hutton, 1994). Total dose rates and resulting OSL ages are summarized in Table 1.

Both physical and biochemical indicators of environmental conditions were examined to infer palaeoenvironmental processes. Grain size was measured by dry sieving, with mean grain size (Mz) and standard deviation (σ) calculated according to the method of Folk and Ward (1957). Colour was first observed and recorded in the field under direct sunlight and then compared to the digital Munsell chart in the laboratory after the samples were dried. Magnetic Susceptibility (MS) was measured with a Bartington MS2 susceptibility metre with a calibration accuracy of ±1%. All measurements involved two magnetic fields reading at the frequencies of 470 Hz (low field) and 4700 Hz (high field), respectively, in the laboratory of the Institute of Geology and Geophysics, CAS, and the unit of mass-specific MS expressed in $m^3\ kg^{-1}$ was applied following Dearing (1999). The percentage frequency dependent susceptibility was calculated from these two readings with the value reflecting the presence of ultrafine superparamagnetic ferrimagnetic minerals appearing as crystals produced by biochemical processes in soil (Dearing, 1999).

Although calcite and dolomite are common components of parent materials in many soils in the world, we believe that $CaCO_3$ in the dune sands of Hunshandake is predominately secondary, because mineralogical studies of the dune sands in the Hunshandake do not show any significance of such minerals due to the overwhelming dominance of quartz and feldspar and a small amount of heavy minerals in the mineralogical compositions (Yang et al., 2007). In our study the content of calcium carbonate was measured with a volumetric calcimeter (Eijkelkamp Corp., Netherlands) that directly determines the production of CO_2 after the sample is mixed with HCl in a closed system under constant pressure and temperature and in the absence of other gases. The error bar for the measurement of the calcium carbonate is less than ±5%.

Total carbon (TC, %) and total organic carbon (TOC, %) were measured with an Elementar Rapid CS Cube that employs a highly-sensitive cuvette multichannel infrared detector to measure the quantities of CO_2 from the combustion of carbon contained in the samples. For preparation, sediment samples were finely ground in

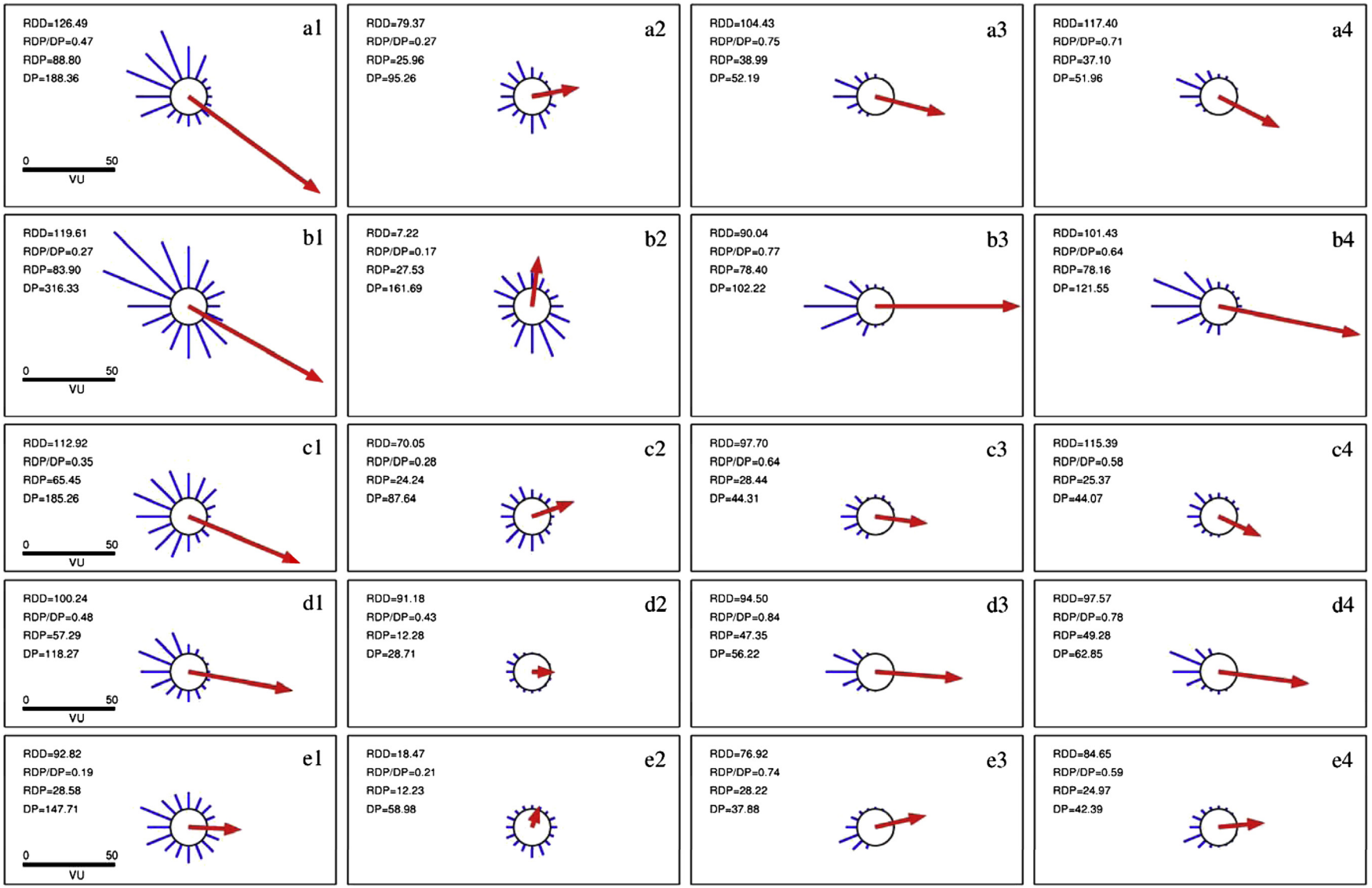

Fig. 3. Sand roses showing sand drift potential on the basis of wind records from the weather stations on the margin of the Hunshandake Sandy Land. a, Erlian Hot; b, Zhurihe; c, Abaga Qi; d, Duolun; e, Xilin Hot (for locations see Fig. 1). Data coverage: 1, spring – March to May; 2, summer – June to August; 3, autumn – September to November and 4, winter – December to February. Sand roses produced using the Fryberger and Dean (1979) method. Wind parameters are described by DP (sand drift potential), RDP (resultant drift potential), RDP/DP (the directional variability) and RDD (the resultant direction of sand movement, 0 referring to the north, clockwise). VU means vector unit with wind speed in knots (Bullard, 1997).

Table 1
Summary data for OSL ages of the samples from the Hunshandake (see Fig. 1 for locations, A – Saihanxili, B – Bayan Nur).

Sample	Depth (m)	U (ppm)	Th (ppm)	K (%)	Water (%)	D (Gy ka^{-1})	*De* (Gy)	Age (ka)
A-1	1.0	0.83	3.68	2.19	10 ± 5	2.66 ± 0.11	10.5 ± 0.1	4.0 ± 0.18
A-2	0.7	0.78	3.13	2.13	10 ± 5	2.57 ± 0.11	8.4 ± 0.1	3.3 ± 0.15
A-3	1.8	0.68	2.91	2.11	10 ± 5	2.47 ± 0.11	23.4 ± 0.4	9.5 ± 0.45
A-4	2.2	0.78	3.29	1.95	10 ± 5	2.36 ± 0.10	31.6 ± 0.6	13.4 ± 0.62
A-5	3.0	0.59	2.42	2.17	10 ± 5	2.45 ± 0.11	29.3 ± 0.6	12.0 ± 0.59
B-1	0.5	0.63	2.76	2.15	10 ± 5	2.56 ± 0.11	2.7 ± 0.1	1.0 ± 0.06
B-2	0.8	0.88	3.96	2.06	10 ± 5	2.58 ± 0.11	3.7 ± 0.1	1.4 ± 0.06
B-3	1.1	0.92	4.21	2.14	10 ± 5	2.66 ± 0.11	8.8 ± 0.1	3.3 ± 0.15
B-4	1.5	0.83	3.35	1.85	10 ± 5	2.30 ± 0.10	23.2 ± 0.3	10.1 ± 0.45
B-5	1.8	0.64	2.42	1.72	10 ± 5	2.07 ± 0.09	26.4 ± 0.3	12.7 ± 0.58
B-6	2.2	0.69	2.60	1.64	10 ± 5	2.01 ± 0.09	25.6 ± 0.3	12.7 ± 0.57
B-7	2.5	0.73	3.21	1.35	10 ± 5	1.78 ± 0.07	22.4 ± 0.3	12.6 ± 0.54
B-8	2.7	0.83	3.02	1.68	10 ± 5	2.09 ± 0.09	42.0 ± 0.5	20.1 ± 0.88
B-9	2.9	0.96	3.86	1.73	10 ± 5	2.22 ± 0.09	28.6 ± 0.5	12.9 ± 0.57

an agate mortar until the bulk samples could be sieved through a 63 μm sieve (Tyler standard 250 mesh). Following the manufacturer's instruction, after combustion at 950 °C the carbon in the samples was fully converted to CO_2 and the percentage of total carbon was calculated. The portion of the powdered sample designated for measuring the content of TOC were first treated with 18% hydrochloric acid to dissolve inorganic carbon and then dried. After the inorganic carbon portion was removed the procedure for measuring TOC with the CS Cube was identical with that for examining TC. The Rapid CS Cube semi-automatically yields the TC and TOC concentrations of the samples with a relative analytical error (relative standard deviation) less than ±1%.

4. Results

4.1. Stratigraphy and chronology

Although the topsoil on the dunes (excluding the lower interdune flats) in the entire Hunshandake looks quite similar to the dune sand of the region, the sections we studied show clear stratigraphic variation in colour in the field, indicating distinct changes in sedimentary conditions in the past. In the SX section there are three different layers separated by a dark layer (9.5–9.7 YR 5–7/4–8) in the middle that is a typical palaeosol in the aeolian sequence (Fig. 4). The underlying part consists of white – yellow (0–3.5 Y 8–9/4–8) aeolian sand, and the uppermost layer is again aeolian sand with a light yellow colour (4–9 Y 7–9/6–8).

Five OSL ages were obtained from the transitional points of the SX section. The basal sand was deposited ca 12–13 ka. Although the dating results of sample A-4 and A-5 seem to suggest a chronological inconsistency (Table 1, Fig. 4), we assume that the base is around 13 ka due to the error bars and uncertainties in the OSL ages. The formation of the palaeosol began at ca 9.5 ± 0.45 ka and ended at ca 4.0 ± 0.18 ka. Based on the OSL chronology, the mean sedimentation rate was calculated and shows a clearly lower rate during the development of the palaeosols (Fig. 5).

With respect to change in sedimentary facies, there is a great similarity between the sections SX and BN. The black brown (6–7 YR 2–7/2–7) palaeosol at BN occurs in the upper part of section and its formation, according to our OSL results (Fig. 4), began at approximately 10.1 ± 0.45 ka, and lasted until 3.3 ± 0.15 ka. There is a transitional layer from the palaeosols to the overlying aeolian sands that is yellow (5–7 YR 4–7/6–8), indicating an increase in aeolian activity upwards. The lower sand layer is a dull yellow (9 YR 7/6) in general, marked by a very coarse sand that is obviously different from the overlying layers. The lowest portion of this sand is particularly coarse and poorly sorted (Figs. 4 and 5), suggesting possible shoreline or fluvial origins. Well consolidated silt and clay underlie this lower coarse sand unit, and were most likely, according to our field observations and judgement, deposited by lacustrine processes. Based on our OSL chronology the period of palaeosol formation experienced a particularly low sedimentation rate in this section (Figs. 4 and 5). We note for consistency that the age of the sample B-8 is not considered in the chronology because it does not fit into the general framework of other ages (Table 1 and Fig. 4).

4.2. Changes of palaeoenvironmental proxies during the last 13,000 years

Our field observation of the stratigraphical changes between palaeosol and aeolian sandy layers is generally supported by physical

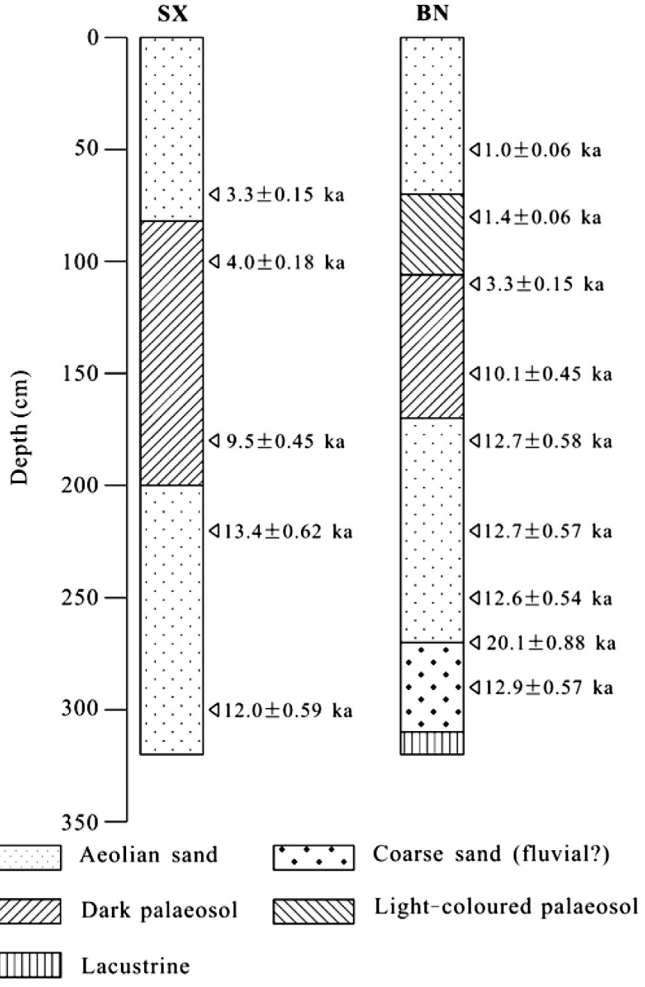

Fig. 4. Stratigraphy and OSL ages of the SX (Saihanxili) and BN (Bayan Nur) sections.

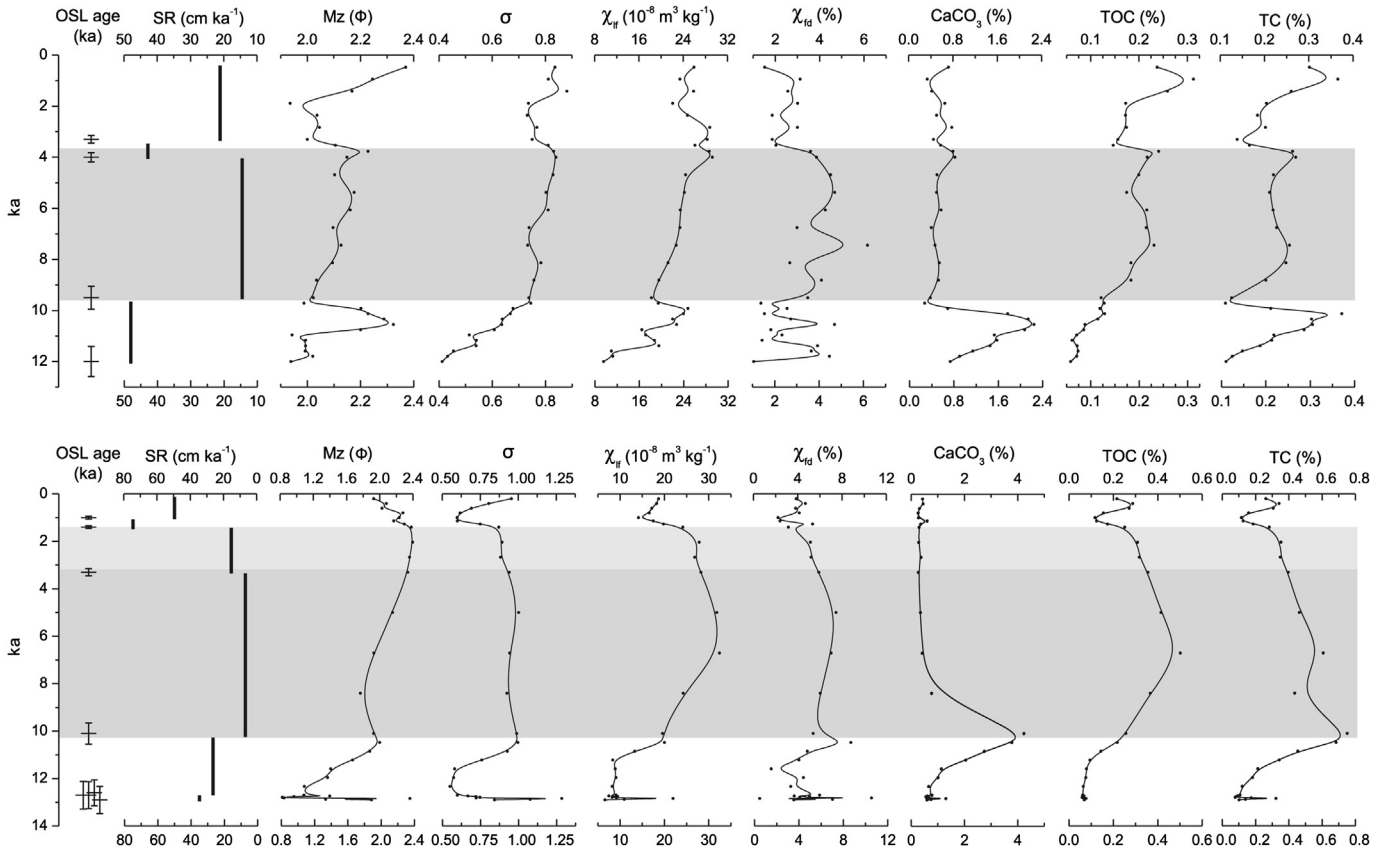

Fig. 5. Mean sedimentation rate (SR), mean grain size (Mz), standard deviation of the grain size distribution (σ), low field magnetic susceptibility (χ_{lf}), frequency susceptibility (χ_{fd}), contents of calcium carbonate, TOC and TC plotted against time scale (linearly interpolated on the basis of the OSL ages) for the Saihanxili (upper) and Bayan Nur (lower) sections. The darker shading marks the period of the palaeosol formation while the light shading indicates transitions between palaeosols and aeolian sands.

and chemical proxies for the palaeoenvironmental reconstruction. Changes in palaeoenvironmental proxies on a linear time scale reveal that the environmental history of the last 13 ka can be divided into three different epochs in both sections (Fig. 5). These conclusions are broadly consistent with our field observations of stratigraphic alteration in the SX and BN sections. However, some proxies, i.e., grain size, magnetic susceptibility, carbon and $CaCO_3$ content, do not exactly follow the same trend, probably due to different key impact factors. In particular, there is no obvious distinction between palaeosols and dune sand in terms of grain size (Fig. 5).

In general there is a good correlation between changes of TC and those of TOC and $CaCO_3$ in both sections. TC and TOC are very low in the portion of the sands underlying the palaeosols, increase abruptly in palaeosols, and decrease again in the sand overlying the palaeosols. At the SX section, the distinctly black brown palaeosol horizon is characterized by a high value of TOC, although TC is lower than that in the underlying aeolian sand (Figs. 4 and 5) which has the lowest organic carbon content in the entire section. The TOC of this dune sand layer is less than 0.10% with just two exceptions where the samples' TOC are 0.13%. In the lower part of the 'modern' aeolian sand layer the TC and TOC are lower, but quite high in depth around 20 cm below the surface (Figs. 4 and 5) possibly due to the impact of modern soil development. Similar to the SX section, the top layer of aeolian sand in the BN section experienced a clear decrease in TOC and TC although the values are higher again at the depth ca 20 cm below the surface. The underlying sand layer contains much less carbon (both TC and $CaCO_3$) and exhibits a lower magnetic susceptibility (Figs. 4 and 5).

Frequency magnetic susceptibility (%) is considerably higher in the palaeosol beds than in the aeolian sands at SX, but the trend is not as clear in the BN section, although the average values of palaeosols are still slightly higher. The mass-specific magnetic susceptibility is generally higher than 20×10^{-8} m^3 kg^{-1} in the palaeosols of the section BN, but lower than 10×10^{-8} m^3 kg^{-1} in the aeolian sand underlying the palaeosols, and between 10 and 20×10^{-8} m^3 kg^{-1} in the sands overlying the palaeosols. However, at SX variations in mass-specific magnetic susceptibility does not show a clear regularity, although it increases slightly upwards (Fig. 5).

5. Discussion

5.1. Environmental changes in the Hunshandake Sandy Land since the late Pleistocene

The occurrence of many shallow basins surrounded by dunes in the Hunshandake suggests distinct variations of the hydrological conditions in the region, and the appearance of lacustrine sediments at an elevation of 1090 m asl. (see Fig. 1) suggests that the entire western portion of the Sandy Land might have been inundated under a single lake in the late Quaternary, consistent with the regional geomorphic feature revealed in digital elevation models (Yang et al., 2011). Although the chronology of the lacustrine sediments we observed at 1090 m has not yet been established, we believe that the timing of this large lake would appear to be ~12 to 13 ka considering the coarse sand (fluvial or shoreline deposits) at the bottom of the BN section and the white sand with a

water-washed appearance at the SX location (Fig. 4). We do not think the coarse sand was a deflation lag on the basis of its facies nature, grain size parameters (Fig. 5) and its location near the lake Bayan Nur. The entire Hunshandake was likely frozen during the LGM because continuous permafrost occurred even in areas 4° to the south, i.e., at the latitude of 38° (Vandenberghe et al., 2004). The large quantity of water required to support the subsequent formation of this large lake could have been sourced from the rivers with head waters in the southern mountains at the later stage of post-LGM global deglaciation (Fig. 1). We believe that the current dunes in the western Hunshandake are probably of late Pleistocene age because of the occurrence of a single large lake prior to the formation of dune landscape, rather than Pliocene as suggested by Li and Dong (1998).

Although aeolian sand accumulation indicates active aeolian activity, removal of sedimentary records is an initial part of the geomorphological processes due to deflation in an aeolian system. This leads to the fact that OSL age frequency histograms from aeolian sand sequences probably show data of sampling frequency rather than likelihood of aeolian accumulation induced by dry climates (Thomas, 2011 and references therein). Therefore our present reconstruction of the environmental changes considers primarily changes in sedimentary facies rather than accumulation rate. The initial appearance of the palaeosols in the sedimentary sections can be interpreted as a sign for the beginning of a post-Pleistocene increase in precipitation and temperature. However, only a decrease in precipitation would be essential to the termination of palaeosol formation in this region. According to our OSL ages at SX palaeosol formation was initiated at ca 9.6 ka, while at BN the palaeosols began forming slightly earlier, i.e., at ca 10.2 ka. Based on the difference in mean annual precipitation between the two sites (currently decreasing 300 mm from east to west across the Hunshandake, Fig. 2), it is quite possible that the post-Pleistocene climate change was time transgressive across the region and that conditions improved slightly earlier at BN than at SX. Considering the obvious precipitation changes within the Hunshandake (Fig. 2), we came to the conclusion that the wetter climate began earlier in the east than in the west. However, since the slight difference in ages is actually within the error bar of the OSL dating, it is also possible that the significant increase in moisture began no later than around 9.6 ka for the entire Hunshandake, regardless of the regional difference. Before palaeosol formation our evidence shows that the region was controlled by aeolian environmental conditions with deposition of aeolian sands suggesting a drier climate in the region that was preceded by a large lake. We interpret such abrupt alteration of environmental conditions as evidence that the regional ecosystem is very sensitive to regional climate change and responds quickly to such change.

Our new date of the initiation of palaeosol formation suggests an earlier start to the Holocene optimum climate in this region. Our interpretation of the beginning of the increased moisture is broadly consistent with the findings from palaeo-spruce timber in the southern Hunshandake. This timber, radiocarbon dated to 10,040 ± 100 cal yr BP, is indicative of a temperate humid forest from 10 to 9 ka in this region, and is supported by the occurrence of mammal fossils found in the same facies as the timber (Cui et al., 1997).

Although the nature of our OSL chronology cannot provide high-resolution records for palaeoclimatic reconstruction, we assume that the increased moisture availability lasted from 9.6 ka to until around 3 ka due to lack of intercalation of aeolian sand in the sequences. The lower value of average sedimentation during the period of palaeosol formation is another indicator for an increase in moisture availability (Fig. 5). Grain size changes at BN show that palaeosols are slightly finer than sands, but the trend is opposite to that at SX, meaning that aeolian sedimentation was not totally dormant while the palaeosols were forming, although the sedimentation rate was much lower (Fig. 5). This suggests the presence of some active dunes during palaeosol formation in some regions of the Hunshandake. The drier western corner of the Sandy Land would likely be the source of aeolian sands even during the Holocene climate optimum because of the predominance of west and northwest winds across the entire region (Fig. 3).

Nonexistence of fundamental grain size difference between palaeosols and aeolian sands (Fig. 5) confirms both a low level of soil formation and the occurrence of sand accumulation during the period of the palaeosol formation. In addition to the sandy sediments in the palaeosols, thin multiple sand layers in association with intermittent accumulation events have been reported in the palaeosols of aeolian sequences in the Hunshandake (Mason et al., 2009) and in other sandy regions, for example, the Nebraska Sand Hills of the USA (Goble et al., 2004). However, it is possible that the palaeosols were developed in the aeolian sands that were deposited by earlier events. In such a case the OSL ages of the palaeosols would be older than the inception of the soil formation. At the same time sands in palaeosols can also be easily reworked by bioturbation, causing younger OSL ages than the true timing for the beginning of the pedogenesis. Considering both directions of the OSL age uncertainties, we think the OSL ages obtained from palaeosols should still fall within the period of pedogenesis.

Bearing in mind that both aeolian sands and layers of palaeosols might be eroded by subsequent deflation, we selected sections with the longest duration of palaeosol formation to reconstruct the regional histories of environmental changes. This is based on the rationale that palaeosols in aeolian sequences are associated with an increase in precipitation and/or the ratio between precipitation and evaporation. For instance, various sequences have been reported from the site Sanggendalai near the southern margin of the Hunshandake (e.g., Li et al., 2002; Yang et al., 2008; Zhou et al., 2008). While Yang et al. (2008) and Zhou et al. (2008) showed thin layers of palaeosols, Li et al. (2002) reported a section where the palaeosols was the thickest layer whose age was dated to between ca 9.8 ka and ca 3.5 ka. For this site we think that the palaeosols were typical in the entire period from ca 9.8 ka to ca 3.5 ka although we personally did not find this specific section.

The termination of optimal Holocene climate conditions in the Hunshandake requires further confirmation also because our two sections are not fully consistent. At Saihanxili the upper boundary of the dark palaeosol is dated to around 4.2 ka. Although the upper boundary of the palaeosols in the BN section was OSL dated to ca 1.4 ca, the optimal climate period ended probably at around 3 ka here because of what we interpreted as the transitional nature of the boundary (Fig. 4). The upper portion of the palaeosol contains a much lower level of TOC and TC as well as a lower magnetic susceptibility (Fig. 5), indicating the onset of drier conditions. We should also mention that our new interpretation is broadly consistent with earlier conclusions in the way that the formation of the mid-Holocene palaeosols was replaced by sand accumulation at the time between ca 4 ka and ca 2 ka dependent on the location of the sections (e.g., Li et al., 2002; Lu et al., 2005; Yang et al., 2008; Zhou et al., 2008).

5.2. Increased mean annual rainfall during the period of palaeosol formation

The relatively high content of calcium carbonate in the lower portion of both sections might be seen as evidence for lower annual precipitation in the semi-arid Hunshandake (Fig. 5). Samples from dune surfaces show that the percentage of calcium carbonate declines from west to east in the desert belt of northern China, consistent with the presently increasing trend of mean annual

precipitation eastwards (Yang et al., 2012). Hövermann (1988) found out that the critical values of mean annual precipitation for forming calcareous cementation via pedogenic processes in African arid landscapes were between 100 and 300 mm, since the calcium carbonate content would rapidly decline due to leaching in areas where mean annual precipitation is over 300 mm. Geographically, it appears there is no clear correlation between the rates of pedogenic accumulation of carbonate and the quantity of regional rainfall in the southern Great Basin of the USA where the mean annual precipitation varies between 80 and 400 mm, since the carbonate content in the parent materials varies greatly from site to site. In the southern Great Basin, however, temporal variation of the carbonate accumulation rate in a same site shows that the Holocene rate was much higher than the rate of later Pleistocene period characterized by cooler and effectively wetter climates (Harden et al., 1991). Studies in the Mojave Desert of the USA demonstrate that pedogenic processes in deserts are dependant on several parameters including fine-sediment availability, climate, vegetation, and the complicated linkages among these parameters (Wells et al., 1987).

Although the mechanism causing changes of magnetic susceptibility may vary from case to case, magnetic susceptibility of aeolian sequences is widely used as a climatic proxy to infer palaeoenvironmental change. The processes causing variations of magnetic susceptibility in the aeolian sands and palaeosols of the Hunshandake would likely be similar to those triggering changes in the loess–palaeosol sections of the Chinese Loess Plateau although specific studies in the sand seas in this regard are still not available. In the Luochuan section of the central Loess Plateau, the low field susceptibility of the palaeosols is about twice that of loess layers (Heller and Liu, 1982). In some other sections the difference of magnetic susceptibility between soil and loess layers is even larger (e.g., An et al., 1991; Maher and Thompson, 1995; Meng et al., 1997; Han and Jiang, 1999). Pedogenesis (e.g., Maher and Thompson, 1995) and decomposition of plants (Meng et al., 1997) can cause magnetic enhancement in palaeosols although other processes such as leaching of carbonate would also have a similar impact (Heller and Liu, 1984). Although the accumulation of nano-sized magnetic particles would generally stay consistent through time, during periods of high aeolian dust sedimentation, as during the formation of loess layers, magnetic grains could be diluted by other particles (Kukla et al., 1988).

The higher frequency dependent susceptibility at SX (Fig. 5) may indicate an increase in biochemical activity in this layer, which is likely associated with an increase in local rainfall and possibly temperature. Although such a tendency is less distinct at the BN section, the frequency dependent susceptibility is still generally higher in the palaeosol layer than in the sands. The higher value at the bottom of this section may arise from dilution (leaching of carbonate) because this layer was probably in a saturated condition in the past.

On a global scale the low-field magnetic susceptibility of bulk surface soil samples is proportionally related to the mean annual rainfall through pedogenesis and it has been found that within a mean annual precipitation range between 200 mm and 1000–1200 mm yr^{-1} MS increases with increasing rainfall (Balsam et al., 2011). This general rule can be used to decipher wetness changes at BN, with the clear increase of MS in the palaeosol layer indicating an increase in mean annual rainfall during the period of palaeosol formation, regardless of the trend in temperature change. This tendency could also be true at SX since MS is lower in the sand layer underlying the palaeosols. Balsam et al. (2011) reported that pedogenic production of ferrimagnets should commence when mean annual rainfall exceeds ~ 200 mm yr^{-1}. However, since local and regional equations relating MS and rainfall are required to estimate rainfall, it is currently impossible to quantitatively assess the changes of mean annual rainfall in the sections due to the lack of a local equation. We believe that our future work will remedy this shortcoming.

Numerical experiments with a comprehensive Earth system model have allowed quantitative understanding of the difference in climate parameters between 6 ka and the present-day monsoonal Asia (Dallmeyer et al., 2010). Since the Hunshandake is located just to the southwest of the test area for Dallmeyer et al.'s (2010) numerical experiments, we believe the simulation is relevant to our study area. The numerical simulation for the area east of the Hunshandake indicates that the annual average precipitation anomalies were 0.1–0.5 mm/day between 6 ka and the present-day (Dallmeyer et al., 2010). In other words, the increase in the mean annual precipitation would have been between 36 and 180 mm in areas located in the northeast. A decrease of 0.5 k was suggested for the mean annual temperature because the increase in temperature would occur only in summer and autumn at 6 ka according to this simulation. Considering the results from this simulation, we assume that the mean annual precipitation increase in the Hunshandake at 6 ka was probably much less than 180 mm because of the greater distance to the moisture source. Using this analogue the maximal mean annual precipitation would be much less than 300 mm in the western margins of Hunshandake, suggesting that some dunes in these marginal areas would be still active at 6 ka. In contrast to our results, a climatic deterioration trend starting at 6100 cal. yr BP was suggested from cores from two small lakes located ca 100 km south of the Hunshandake, while the wettest period was interpreted as occurring from 9.6 to 7.6 ka (Wang et al., 2011).

5.3. Regional comparisons and forcing

With respect to the regional correlation of late Quaternary dune activity, two issues are of particular importance. First, the activity of a single dune is not equal to that of an entire dune field in semi-arid regions (Muhs and Holliday, 1995; Werner et al., 2011). Even at the present time, and often due to large differences between windward and lee sides, it is a challenging task to assess the stability of dunes in Hunshandake. In this context, we have just considered the occurrence of palaeosols as an indicator of fixation on the dune surface because the formation of soil must be related to a sustainable occurrence of vegetative cover. Second, the extension and size of dunes in the sandy lands of northern China varies greatly (Yang et al., 2012) and climate parameters required to stabilize this range of dunes may not be the same (Lancaster, 1988, 1995; Embabi, 2004; Fitzsimmons et al., 2007; Cohen et al., 2010).

In general, the episodic nature of Late Quaternary dune activity has been reported for all sandy lands in the eastern part of the desert belt in northern China, with large-scale stabilization of dunes occurring in the middle Holocene (Fig. 6). It has even been suggested that the desertification in these areas was mainly triggered by human activity at more recent times (Zhu and Liu, 1981). The availability of old aeolian sand is, of course, conducive to the new appearance of dunes in this region. A temporal framework of dune instability in northern China emerges after the dates from various regions are compiled, although the palaeoclimatic interpretation of each aeolian record needs to be considered with respect to onsite details (Fig. 6). In addition, significant uncertainty still exists with regard to the initial timing of the large-scale dune stabilization in the sandy lands. In contrast with our interpretation of the BN and SX sections in the Hunshandake, Mason et al. (2009) reported that dunes in the sandy lands of China were still active during the earlier Holocene (11.5–8 ka). Even during the period between 8 and 6 ka, sand mobility was not rare in these sandy

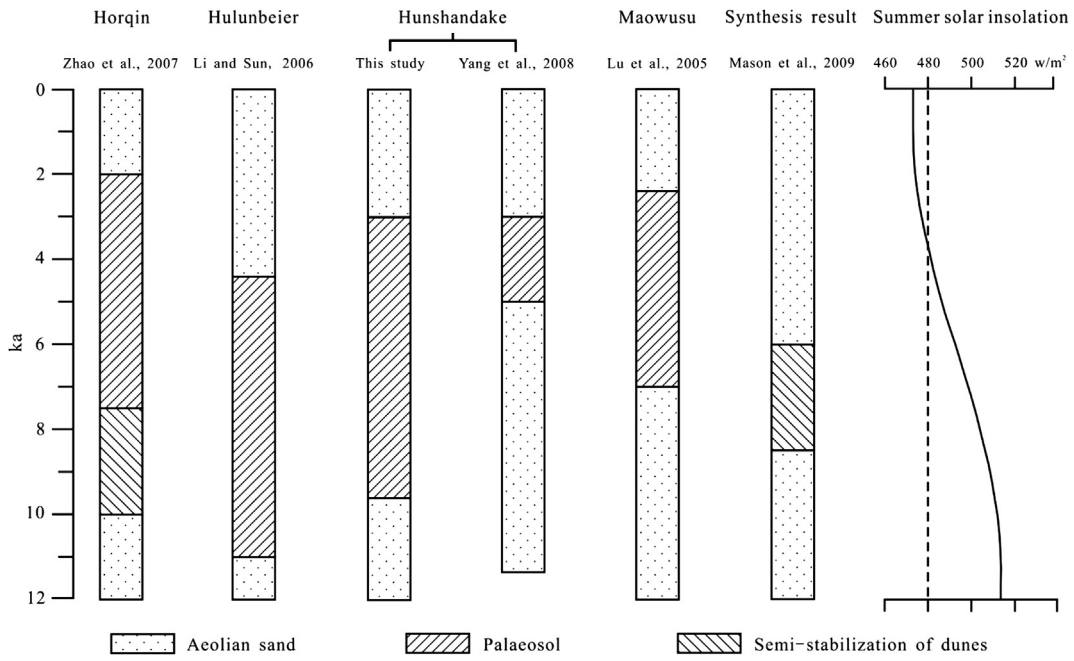

Fig. 6. OSL chronologies of the Holocene climate optimum inferred from palaeosols in aeolian sequences in the eastern portion of the desert belt in northern China (for location of each dune field see Fig. 7) compared with the Holocene changes of summer (May–September) solar insolation at 40°N (Berger and Loutre, 1991).

lands according to their OSL chronologies (Mason et al., 2009). Taking the Hunshandake as an example, it is reasonable to assume that isolated active dunes would still occur in the western part of the Maowusu (Mu Us) also during the period of Holocene optimal climate.

An even longer period of stabilization occurred during the early and middle Holocene in the dune fields located east of the Hunshandake. The largest sandy land, the Horqin, is characterized by the occurrence of source-bordering dunes. The lateral migration of channels is crucial to the dune formation in the Horqin as this process prepared both space and sediments for the aeolian dunes (Han et al., 2007). The dune stabilization and chernozem soil development have been OSL dated to the period between 7.5 ka and 2.0 ka, and the period from 10 ka to 7.5 ka has been attributed to semi-stabilization of the dunes in Horqin (Zhao et al., 2007). In the sedimentary sections of dunes in the Hulunbeier Sandy Land the main feature is a palaeosol intercalated by thin layers of aeolian sand. There the earliest palaeosol OSL date is 12.4 ± 1.2 ka (Li and Sun, 2006). This sandy land probably experienced the longest period of stability due to relatively high annual precipitation (300–400 mm) and higher latitude driven lower temperatures. OSL ages from 11 to ca 4.4 ka (Li and Sun, 2006) support this contention. In the Maowusu Sandy Land there is evidence for active dunes from 13 to 6 ka (Mason et al., 2009), although soil development in the eastern part of the Maowusu was dated to the period between 7 and 2.4 ka (Lu et al., 2005).

Considering the general nature of glacial–interglacial climate changes (Liu, 2009), it is reasonable to assume that the largest extension of dune fields in the eastern portion of the desert belt in northern China would have occurred at the Last Glacial Maximum (LGM), although little stratigraphic evidence and physical dating of sand from the LGM has been obtained from the region to date. Although there is a general absence of chronological evidence for sand deposition at the time around Last Glacial Maximum (21 ka) in the sandy lands, we still conclude that there might have been a widespread extension of sand seas (mainly active dunes) in this region due to globally colder, windier and drier conditions. Since the sand seas are considered to be sources of loess in China, this is consistent with the high accumulation rate of loess during glacials in many loess–palaeosol sections (Liu, 2009). We, however, do not think that the extension of the sand seas was much beyond the area where sandy sediments occur today. Compared with the overwhelmingly stabilization of dunes during the middle Holocene, the present extension of the dune fields is an intermediate state (Fig. 7).

When compared with sandy lands in the eastern portion of the desert belt, the sand seas of western China should have experienced significantly less change in terms of geographical extension around the LGM, the mid-Holocene and at present due to the generally arid climate (Fig. 7). However, the nature of each dune field may vary greatly and rapidly in response to regional, global climate changes and to regional hydrological fluctuation (Yang et al., 2011). For example, the increase in precipitation during the middle Holocene in the Badain Jaran Desert caused a significant increase in lake levels of interdune lakes and large extension in the area of wetlands in interdune basins (Yang and Williams, 2003; Yang et al., 2010), but was probably not sufficiently wet to fully stabilize the slopes of the dunes. Therefore, we think the large sand seas in western China were parts of active dune fields even during the mid-Holocene although wetlands and vegetated areas within the dune fields might have increased considerably (Fig. 7). An overall enlargement of the sand seas during the LGM was probably not likely in western China (Fig. 7), either, due to the multiple parameters controlling the formation of sand seas rather than just aridity (Yang et al., 2012). Referring to the ratios between precipitation and evaporation (P/E), numerical simulations show that the climate might have been even wetter during the LGM in the desert areas of western China (Jiang et al., 2011), a result broadly consistent with the interpretations of lacustrine and geomorphological records from the desert regions (Yu et al., 2003; Yang and Scuderi, 2010; Yang et al., 2003, 2011).

Orbital forcing via changes of solar radiation would be the key cause for the environmental changes in the deserts of northern China although there is a long time lag between the increase in

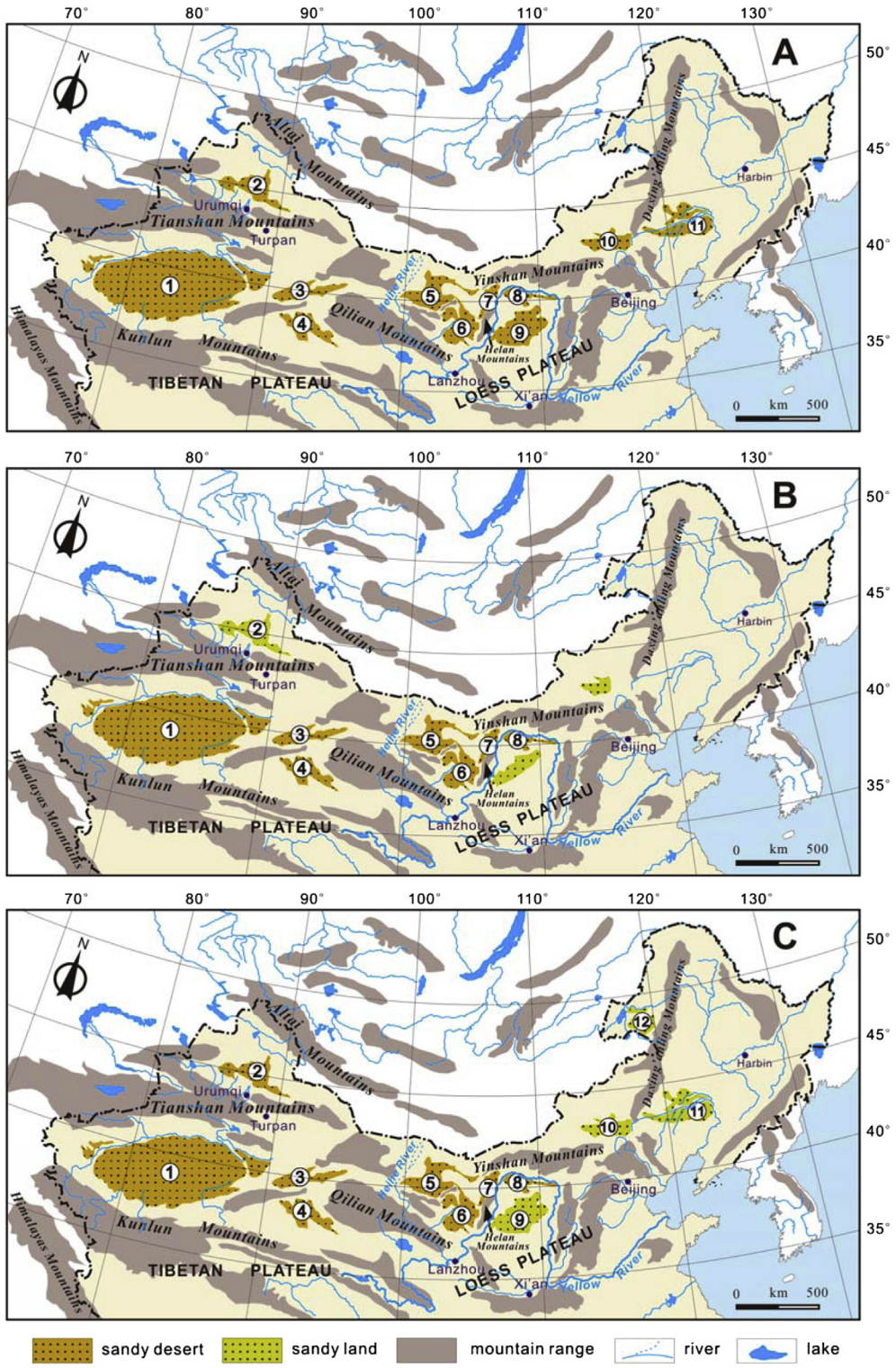

Fig. 7. General distribution patterns of dune fields in northern China at the (A) LGM, (B) Holocene climate optimum at ca 6 ka and (C) present. Sandy deserts (active dune fields) and sandy lands (fields of stabilized dunes) are indicated with numbers. Individual deserts and sandy lands key: 1, Taklamakan; 2, Gurbantunggut; 3, Kumtag; 4, Chaidamu; 5, Badain Jaran; 6, Tengger; 7, Wulanbuhe; 8, Kubuqi; 9, Maowusu; 10, Hunshandake; 11, Horqin; 12, Hulunbeier. Sources of the data: Map C was modified from Yang et al. (2012) with initial data in Zhu et al. (1980); Map B was drawn on the basis of the synthesis of the various records discussed in 5.3 and Map A was drawn considering a generally colder, windier and drier environment during the LGM in the deserts of northern China (e.g., Williams et al., 1998; Goudie, 2002; Vandenberghe et al., 2004; Liu, 2009; Yang and Scuderi, 2010; Yang et al., 2011).

solar radiation and occurrence of palaeosols (Fig. 6). This is likely related to a temporal factor that would require at least 10^3 years to transfer one type of landscape to another in the sense of climatic geomorphology (Hövermann, 1985). Mason et al. (2009) suggested that the drier climate in the early Holocene was due to a dynamic link between enhanced diabatic heating in the core region of the strengthened monsoon and increased subsidence in the drylands to the north, and as a result of high summer temperatures.

6. Conclusions

Deserts in the eastern portion of Asian mid-latitude desert belt are quite different from those in the western portion in terms of stability, landforms and late Quaternary history. Although aridity in the region has a long history, the current desert landscape in the eastern portion can only be traced back to the late Pleistocene. The formation of palaeosols in the aeolian sequences in Hunshandake, supported by physical indicators such as magnetic susceptibility and biochemical indicators such as organic and inorganic carbon content, confirm that the dune landscape was stabilized by vegetation to a large degree during the early and middle Holocene probably due to the increase in moisture in association with an increase in solar radiation receipt. The OSL chronology of the two sections we studied suggests that this period was from 9.6 ka to 3 ka. From the observed change in the palaeoenvironmental proxies, supported by results from numerical simulations (Dallmeyer et al., 2010), we conclude that the early and middle Holocene was probably characterized by an increase in mean annual precipitation of 30–140 mm, however, the increase in mean annual temperature over the same time scale is still uncertain. Considering the current limited precipitation of the western Hunshandake even with an increase it is quite likely that the western corner of Hunshandake was still undergoing active aeolian processes while other parts of the Sandy Land were covered by vegetation. Our analysis of the various aeolian sequences leads further to the conclusion that periods of Holocene dune stabilization varied and in general it began earlier and lasted longer in the east than in the west in the sandy lands of northern China according to the records of the palaeosols. The reactivation of the dunes during the last 3000 years is partly from an aridification trend as shown in the aeolian sequences and is probably related to the decrease in the intensity of East Asian summer monsoon in response to the decrease in solar radiation, broadly consistent with the palaeoenvironmental histories of other sandy lands in northern China.

Acknowledgements

This collaborative research was supported by the National Natural Science Foundation of China (Grant nos.: 40930105, 41172325) and the CAS Strategic Priority Research Program (Grant no. XDA05120502). We thank the Chinese Meteorological Agency for providing weather data, Prof. Nick Lancaster and two anonymous reviewers for their constructive comments on earlier drafts of this manuscript.

References

Adamiec, G., Aitken, M., 1998. Dose-rate conversion factors: update. Ancient TL 16, 37–50.
An, Z., Kukla, G.J., Porter, S.C., Xiao, J., 1991. Magnetic susceptibility evidence of monsoon variation on the Loess Plateau of central China during the last 130,000 years. Quaternary Research 36, 29–36.
An, Z., Porter, S.C., Kutzbach, J.E., Wu, X., Wang, S., Liu, X., Li, X., Zhou, W., 2000. Asynchronous Holocene optimum of the East Asian monsoon. Quaternary Science Reviews 19, 743–762.
Balsam, W.L., Ellwood, B.B., Ji, J., Williams, E.R., Long, X., Hassani, A.E., 2011. Magnetic susceptibility as a proxy for rainfall: worldwide data from tropical and temperate climate. Quaternary Science Reviews 30, 2732–2744.
Berger, A., Loutre, M., 1991. Insolation values for the climate of the last 10 million years. Quaternary Science Reviews 10, 297–317.
Bullard, J., 1997. A note on the use of the "Fryberger method" for evaluating potential sand transport by wind. Journal of Sedimentary Research 67, 499–501.
Cohen, T.J., Nanson, G.C., Larsen, J.R., Jones, B.G., Price, D.M., Coleman, M., Pietsch, T.J., 2010. Late Quaternary aeolian and fluvial interactions on the Cooper Creek Fan and the association between linear and source-bordering dunes, Strzelecki Desert, Australia. Quaternary Science Reviews 29, 455–471.
Cui, H., Liu, H., Yao, X., 1997. The finding of a paleo-spruce timber in Hunshandak sandy land and its paleoecological significance. Science in China (Series D) 40, 599–604.
Dallmeyer, A., Claussen, M., Otto, J., 2010. Contribution of oceanic and vegetation feedbacks to Holocene climate change in monsoonal Asia. Climate of the Past 6, 195–218.
Dearing, J.A., 1999. Environmental Magnetic Susceptibility: Using the Bartington MS2 System. Bartington Instruments Limited, Oxford.
Derbyshire, E., Goudie, A., 1997. Asia. In: Thomas, D. (Ed.), Arid Zone Geomorphology, second ed. Wiley, Chichester, pp. 487–506.
Domrös, M., Peng, G., 1988. The Climate of China. Springer-Verlag, Berlin Heidelberg New York.
Embabi, N.S., 2004. The Geomorphology of Egypt: Landforms and Evolution. In: The Nile Valley and the Western Desert, vol. I. The Egyptian Geographical Society, Cairo.
Fitzsimmons, K.E., Rhodes, E.J., Magee, J.W., Barrows, T.T., 2007. The timing of linear dune activity in the Strzelecki and Tirari Deserts, Australia. Quaternary Science Reviews 26, 2598–2616.
Folk, R., Ward, W., 1957. Brazos river bar: a study in the significance of grain size parameters. Journal of Sedimentary Petrology 27, 3–26.
Fryberger, S.G., Dean, G., 1979. Dunes forms and wind regime. In: McKee, E.D. (Ed.), A Study of Global Sand Seas. Geological Survey Professional Paper, vol. 1052. U.S. Government Printing Office, Washington, pp. 137–170.
Goble, R., Mason, J., Loope, D., Swinehart, J., 2004. Optical and radiocarbon ages of stacked paleosols and dune sands in the Nebraska Sand Hills, USA. Quaternary Science Reviews 23, 1173–1182.
Goudie, A.S., 2002. Great Warm Deserts of the World: Landscapes and Evolution. Oxford University Press, New York.
Han, J., Jiang, W., 1999. Particle size contributions to bulk magnetic susceptibility in Chinese loess and paleosol. Quaternary International 62, 103–110.
Han, G., Zhang, G., Dong, Y., 2007. A model for the active origin and development of source-bordering dunefields on a semiarid fluvial plain: a case study from the Xiliaohe Plain, Northeast China. Geomorphology 86, 512–524.
Harden, J., Taylor, E., Hill, C., Mark, R., McFadden, L., Reheis, M., Sowers, J., Wells, S., 1991. Rates of soil development from four soil chronosequences in the southern Great Basin. Quaternary Research 35, 383–399.
Heller, F., Liu, T., 1982. Magnetostratigraphical dating of loess deposits in China. Nature 300, 431–433.
Heller, F., Liu, T., 1984. Magnetism of Chinese loess deposits. Geophysical Journal of the Royal Astronomical Society 77, 125–141.
Hövermann, J., 1985. Das System der klimatischen Geomorphologie auf landschaftskundlicher Grundlage. Zeitschrift für Geomorphologie Supplementband 56, 143–153.
Hövermann, J., 1988. The Sahara, Kalahari and Namib deserts: a geomorphological comparison. In: Dardis, G., Moon, B. (Eds.), Geomorphological Studies in Southern Africa. Balkema, Totterdam, pp. 71–83.
Jiang, D., Lang, X., Tian, Z., Guo, D., 2011. Last Glacial Maximum climate over China from PMIP simulations. Palaeogeography, Palaeoclimatology, Palaeoecology 309, 347–357.
Köppen, W., 1931. Grundrisse der Klimakunde. Walter de Gruyter, Berlin.
Kukla, G., Heller, F., Liu, X., Xu, T., Liu, T., An, Z., 1988. Pleistocene climates in China dated by magnetic susceptibility. Geology 16, 811–814.
Lancaster, N., 1988. Development of linear dunes in the southwestern Kalahari, Southern-Africa. Journal of Arid Environments 14, 233–244.
Lancaster, N., 1995. Geomorphology of Desert Dunes. Routledge, London.
Li, X., Dong, G., 1998. Preliminary studies on the age and formation of the Hunshandake Sandy Land. Journal of Desert Research 18, 16–21 (in Chinese with English abstract).
Li, S., Sun, J., 2006. Optical dating of Holocene dune sands from the Hulun Buir Desert, northeastern China. The Holocene 16, 457–462.
Li, S., Sun, J., Zhao, H., 2002. Optical dating of dune sands in the northeastern deserts of China. Palaeogeography, Palaeoclimatology, Palaeoecology 181, 419–429.
Liu, T., 2009. Loess and Arid Environment. Anhui Science and Technology Press, Beijing (in Chinese).
Lu, H., Miao, X., Zhou, Y., Mason, J., Swinehart, J., Zhang, J., Zhou, L., Yi, S., 2005. Late Quaternary aeolian activity in the Mu Us and Otindag dune fields (north China) and lagged response to insolation forcing. Geophysical Research Letters 32, L21716.
Maher, B.A., Thompson, R., 1995. Paleorainfall reconstructions from pedogenic magnetic susceptibility variations in the Chinese loess and paleosols. Quaternary Research 44, 383–391.
Mason, J.A., Swinehart, J.B., Lu, H., Miao, X., Cha, P., Zhou, Y., 2008. Limited change in dune mobility in response to a large decrease in wind power in semi-arid northern China since the 1970s. Geomorphology 102, 351–363.
Mason, J.A., Lu, H., Zhou, Y., Miao, X., Swinehart, J.B., Liu, Z., Goble, R.J., Yi, S., 2009. Dune mobility and aridity at the desert margin of northern China at a time of peak monsoon strength. Geology 37, 947–950.
Meng, X., Derbyshire, E., Kemp, R.A., 1997. Origin of the magnetic susceptibility signal in Chinese loess. Quaternary Science Reviews 16, 833–839.
Muhs, D.R., Holliday, V.T., 1995. Evidence of active dune sand on the great plains in the 19th century from accounts of early explorers. Quaternary Research 43, 198–208.
Murray, A.S., Wintle, A.G., 2000. Luminescence dating of quartz using an improved single-aliquot regenerative-dose protocol. Radiation Measurements 33, 57–73.
Prescott, J.R., Hutton, J.T., 1994. Cosmic ray contributions to dose rates for luminescence and ESR dating: large depth and long time variations. Radiation Measurements 23, 497–500.
Ren, M., 1980. The Outline of Physical Geography of China (Revised Version). Commercial Publisher, Beijing (in Chinese).

Sun, J., Ding, Z., Liu, T., 1998. Desert distributions during the glacial maximum and climatic optimum: example of China. Episode 21, 28–31.
Thomas, D., 2011. Reconstructing paleoenvironments and palaeoclimates in drylands: what can landform analysis contribute? Earth Surface Processes and Landforms http://dx.doi.org/10.1002/esp.3190.
Tooth, S., 2008. Arid geomorphology: recent progress from an earth system science perspective. Progress in Physical Geography 32, 81–101.
Vandenberghe, J., Cui, Z., Zhao, L., Zhang, W., 2004. Thermal-contraction-crack networks as evidence for late-Pleistocene permafrost in Inner Mongolia, China. Permafrost and Periglacial Processes 15, 21–29.
Wang, T., 2003. Desert and Desertification in China. Hebei Science and Technology Press, Shijiazhuang (in Chinese).
Wang, H., Liu, H., Zhao, F., Yin, Y., Zhu, J., Snowball, I., 2011. Early- and mid-Holocene palaeoenvironments as revealed by mineral magnetic, geochemical and palynological data of sediments from Bai Nuur and Ulan Nuur, southeastern inner Mongolia Plateau, China. Quaternary International 250, 100–118.
Warren, A., 1988. The dynamics of network dunes in the Wahiba Sand: a progress report. Journal of Oman Studies Special Report 3, 169–181.
Wells, S.G., McFadden, L.D., Dohrenwend, J.C., 1987. Influence of Late Quaternary climatic changes on geomorphic and pedogenic processes on a desert piedmont, eastern Mojave Desert, California. Quaternary Research 27, 130–146.
Werner, C., Mason, J., Hanson, P., 2011. Non-linear connections between dune activity and climate in the High Plains, Kansas and Oklahoma, USA. Quaternary Research 75, 267–277.
Williams, M., Dunkerley, D., De Deckker, P., Kershaw, P., Chappell, J., 1998. Quaternary Environments, Second ed. Arnold, London.
Wu, G., Liu, Y., Wang, T., Wan, R., Liu, X., Li, W., Wang, Z., Zhang, Q., Duan, A., Liang, X., 2007. The influence of mechanical and thermal forcing by the Tibetan Plateau on Asian climate. Journal of Hydrometeorology 8, 770–789.
Yang, X., Scuderi, L.A., 2010. Hydrological and climatic changes in deserts of China since the late Pleistocene. Quaternary Research 73, 1–9.
Yang, X., Williams, M., 2003. The ion chemistry of lakes and late Holocene desiccation in the Badain Jaran Desert, Inner Mongolia, China. Catena 51, 45–60.
Yang, X., Liu, T., Xiao, H., 2003. Evolution of megadunes and lakes in the Badain Jaran Desert, Inner Mongolia, China during the last 31000 years. Quaternary International 104, 99–112.
Yang, X., Liu, Y., Li, C., Song, Y., Zhu, H., Jin, X., 2007. Rare earth elements of aeolian deposits in Northern China and their implications for determining the provenance of dust storms in Beijing. Geomorphology 87, 365–377.
Yang, X., Zhu, B., Wang, X., Li, C., Zhou, Z., Chen, J., Wang, X., Yin, J., Lu, Y., 2008. Late Quaternary environmental changes and organic carbon density in the Hunshandake Sandy Land, eastern Inner Mongolia, China. Global and Planetary Change 61, 70–78.
Yang, X., Ma, N., Dong, J., Zhu, B., Xu, B., Ma, Z., Liu, J., 2010. Recharge to the interdune lakes and Holocene climatic changes in the Badain Jaran Desert, western China. Quaternary Research 73, 10–19.
Yang, X., Scuderi, L., Paillou, P., Liu, Z., Li, H., Ren, X., 2011. Quaternary environmental changes in the drylands of China – a critical review. Quaternary Science Reviews 30, 3219–3233.
Yang, X., Li, H., Conacher, A., 2012. Large-scale controls on the development of sand seas in northern China. Quaternary International 250, 74–83.
Yu, G., Xue, B., Liu, J., Chen, X., 2003. LGM lake records from China and an analysis of climate dynamics using a modeling approach. Global and Planetary Change 38, 223–256.
Zhao, H., Lu, Y., Yin, J., 2007. Optical dating of Holocene sand dune activities in the Horqin sand-fields in Inner Mongolia, China, using the SAR protocol. Quaternary Geochronology 2, 29–33.
Zhou, Y., Lu, H., Mason, J., Miao, X., Swinehart, J., Goble, R., 2008. Optically stimulated luminescence dating of aeolian sand in the Otindag dune field and Holocene climate change. Science in China Series D 51, 837–847.
Zhu, Z., Chen, G., 1994. Sandy Desertification in China. Science Press, Beijing (in Chinese).
Zhu, Z., Liu, S., 1981. Desertification Processes and their Control in Northern China. China Forestry Press, Beijing (in Chinese).
Zhu, Z., Wu, Z., Liu, S., Di, X., 1980. An Outline of Chinese Deserts. Science Press, Beijing (in Chinese).